www.elsevier.com/locate/memsci

Graphene/PVDF flat-sheet membrane for the treatment of RO brine from coal seam gas produced water by air gap membrane distillation

Yun Chul Woo, Youngjin Kim, Wang-Geun Shim, Leonard D. Tijing, Minwei Yao, Long D. Nghiem, June-Seok Choi, Seung-Hyun Kim, Ho Kyong Shon

PII: S0376-7388(16)30225-3
DOI: http://dx.doi.org/10.1016/j.memsci.2016.04.014
Reference: MEMSCI14414

To appear in: *Journal of Membrane Science*

Received date: 12 December 2015
Revised date: 4 April 2016
Accepted date: 5 April 2016

Cite this article as: Yun Chul Woo, Youngjin Kim, Wang-Geun Shim, Leonard D. Tijing, Minwei Yao, Long D. Nghiem, June-Seok Choi, Seung-Hyun Kim and Ho Kyong Shon, Graphene/PVDF flat-sheet membrane for the treatment of RO brine from coal seam gas produced water by air gap membrane distillation, *Journal of Membrane Science,* http://dx.doi.org/10.1016/j.memsci.2016.04.014

Graphene/PVDF flat-sheet membrane for the treatment of RO brine from coal seam gas produced water by air gap membrane distillation

Yun Chul Woo[a], Youngjin Kim[a,b], Wang-Geun Shim[a,c], Leonard D. Tijing[a,*], Minwei Yao[a], Long D. Nghiem[d], June-Seok Choi[e], Seung-Hyun Kim[f] and Ho Kyong Shon[a,*]

[a]Centre for Technology in Water and Wastewater, School of Civil and Environmental Engineering, University of Technology Sydney (UTS). P. O. Box 123, 15 Broadway, NSW 2007, Australia

[b]School of Civil, Environmental & Architectural Engineering, Korea University, 1-5 Ga, Anam-Dong, Sungbuk-gu, Seoul, 136-713, Republic of Korea

[c]Department of Polymer Science and Engineering, Sunchon National University, 255 Jungang-ro, Suncheon, Jeollanam-do, Republic of Korea

[d]Strategic Water Infrastructure Laboratory, School of Civil Mining and Environmental Engineering, University of Wollongong, Wollongong, NSW 2522, Australia

[e]Environment and Plant Research Institute, Korea Institute of Civil Engineering and Building Technology (KICT), 283, Goyangdae-Ro, Ilsanseo-Gu, Goyang-Si, Gyeonggi-Do, 411-712, Republic of Korea

[f]Civil Engineering Department, Kyungnam University, Wolyoung-dong, Changwon, 631-701, Republic of Korea

[*]Corresponding authors: L.D. Tijing, e-mail: Leonard.Tijing@uts.edu.au, ltjing@gmail.com, Tel: +61 2 9514 2652; H.K. Shon, e-mail: Hokyong.Shon-1@uts.edu.au, Tel: +61 2 9514 2629

Abstract

Brine management of coal seam gas (CSG) produced water is a significant concern for the sustainable production of CSG in Australia. Membrane distillation (MD) has shown the potential to further reduce the volume of CSG reverse osmosis (RO) brine. However, despite its potential, the lack

of appropriate MD membranes limits its industrial use. Therefore, this study was aimed on the fabrication of a robust membrane for the treatment of real RO brine from CSG produced water via an air gap MD (AGMD) process. Here, graphene/polyvinylidene fluoride (G/PVDF) membranes at various graphene loadings (0.1 to 2.0 wt% w.r.t. to PVDF) were prepared through a phase inversion method. Surface characterization revealed that all G/PVDF membranes exhibited favorable membrane properties having high porosity (>78%), suitable mean pore size (<0.11µm), and high liquid entry pressure (>3.66 bar). AGMD test results (feed inlet: 60.0 ± 1.5^{o}C; coolant inlet: 20.0 ± 1.5 ^{o}C) for 24 h operation indicated a high water vapor flux and salt rejection of 20.5 L/m^{2}h and 99.99%, respectively for the optimal graphene loading of 0.5 wt%, i.e., G/PVDF-0.5 membrane (compared to 11.6 L/m^{2}h and 99.99% for neat PVDF membrane). Long-term AGMD operation of 10 days further revealed the robustness of G/PVDF membrane with superior performance compared to commercial PVDF membrane (85.3% final normalized flux/99.99% salt rejection against 51.4%/99.95% for commercial membrane). Incorporation of graphene has resulted to improved wetting resistance and more robust membrane that has the potential for the treatment of RO brine from CSG produced water via AGMD.

Keywords: Graphene/PVDF membrane, CSG produced water, RO brine, air gap membrane distillation, phase inversion

1. Introduction

Coal seam gas (CSG), also known as coal seam methane or coal bed methane, is a natural gas located in the coal seams underground (300 ~ 1,000 m). CSG exploration has recently emerged as a major industry in Australia [1]. The CSG industry is developing quickly responding to the rapid growth of the export business. However, CSG extraction also involves the co-production of a large volume of water, termed as produced water, which is basically saline groundwater. In Australia, CSG produced water is mainly composed of sodium, bicarbonate and chloride [1, 2]. Due to potential impacts of directly discharging CSG produced water on local ecological systems, there is a strong need to develop sustainable treatment process for its environmental safety [1, 3-5]. CSG produced

water requires advanced technologies for treatment such as RO because the salt removal from CSG produced water is a crucial point [4, 6]. Treating CSG produced water with RO leads to the production of more concentrated CSG produced water called brine [1]. The management of this CSG RO brine is a significant concern for the sustainable production of CSG [3]. As policies on the storage and disposal of CSG produced water become more stringent, it is imperative to further reduce the volume of CSG RO brine or to recover some minerals from it as saleable products. One emerging technology that could be utilized to further concentrate the RO brine near saturation is membrane distillation (MD).

In MD, only water vapor is allowed to pass through a barrier, usually a hydrophobic porous membrane and is condensed in the permeate side as pure water. The driving force is the partial vapor pressure difference resulting from the thermal gradient between the hot feed and cool permeate streams [7, 8]. Theoretically, it can reject 100% of the salts and non-volatile components at the feed. One advantage of MD is that it can work at low heating temperature, thus it is possible to utilize solar energy, low grade or waste heat to maintain lower energy consumptions than the conventional distillation systems. Recent studies reported the feasibility of treating many feed water types using MD such as salty water, impaired water resources, and CSG RO brine [3, 9]. Duong et al. [3] has successfully demonstrated a pilot-scale study of a spiral-wound air gap MD to treat CSG RO brine with 80% water recovery. However, MD has still not been fully implemented in industrial level, wherein the lack of an efficient and specially-designed membrane is one of the major reasons. Though the commonly used microfiltration (MF) membranes can be utilized, they still have wetting issues and are of sub-optimal performance. Hence, there is a need to develop new, robust membranes specific for MD process. Ideal MD membranes possess high hydrophobicity, high porosity, adequate pore size and narrow pore size distribution, and good chemical stability.

Phase inversion is a commonly-used technique in fabricating membranes by exposing a homogeneous polymer solution into a non-solvent bath, inverting a single phase into a two-phase system. However, current phase inverted membranes still suffers from low hydrophobicity and low porosity [10], which consequently affect the membrane permeability and rejection. Several membrane design and surface modification techniques have been carried out to enhance the membrane properties

such as plasma treatment [11], addition of pore additives (e.g. polyethylene glycol) [12] and incorporation of inorganic nanoparticles such as clay [13], calcium carbonate [14], CuO [15], carbon nanotube [16, 17] and activated carbon [18]. The addition of nanoparticles is known to affect the morphology, porosity, pore size and mechanical properties of the membrane, and provides additional diffusion pathway. The various modification techniques have led to improvements in MD performance to some extent, but the membrane still suffers from wetting issues and not so high permeate flux. In addition, most of the reported studies only utilized either direct contact MD (DCMD) or vacuum MD (VMD) configurations, and limited themselves on only testing NaCl solution at various concentrations as feed.

In the present study, an air gap MD (AGMD) was employed to treat RO brine from CSG produced water utilizing a composite phase inverted flat-sheet membrane incorporated with graphene nanoparticles. AGMD is better than DCMD process in terms of temperature polarization due to a high heat transfer resistance, which leads to increasing operation duration with stable flux and rejection performances. Graphene, an allotrope of carbon composed of sp^2 bonded atoms arranged in hexagonal lattice, possesses many interesting properties for MD application such as high hydrophobicity, ion selectivity and water vapor transport, good thermal stability and mechanical properties [19, 20]. Graphene has attracted considerable attention in recent years for water treatment and purification processes as it improves the membrane properties and adds functionalities such as anti-fouling properties [21, 22]. The possibility of cheaper synthesis of large area of graphene as recently reported makes it more interesting for modern use [23]. Graphene shows great potential as filler material and is ought to be explored. To the best of our knowledge, this research is the first attempt to fabricate phase inversion composite membranes containing graphene as additives for treatment of RO brine from CSG produced water by AGMD process. The addition of a small amount of graphene in the membrane was expected to improve the membrane hydrophobicity, liquid entry pressure (LEP), porosity, and consequently better flux and salt rejection.

2. Experimental methods

2.1 Material

Polyvinylidene fluoride (PVDF, Kynar® 761, Mw = 441,000 g/mol) was purchased from Arkema Inc., Australia, and N,N-dimethylformamide (DMF) and LiCl were purchased from Sigma-Aldrich. The graphene used in the present study was xGNP-C500-grade materials (XG-Science, USA). It has a nominal diameter of 1 ~ 2 microns, average thickness of 2 nm, and average surface area of 500 m^2/g. Ethanol was purchased from Ajax Finechem Pty Ltd for measuring porosity. For the AGMD performances, sodium chloride (NaCl, Chem-supply) and deionized (DI) water from a Millipore Milli-Q water system were used. All chemicals were used as received. In addition, a commercial PVDF membrane (herein referred to as C-PVDF) (Durapore®-GVHP, pore size of 0.22 μm) was purchased from Merck Millipore for comparison.

2.2 Dope preparation

A neat 10 wt% PVDF solution was prepared by dissolving a certain amount of PVDF powder in DMF solvent with 3 wt% LiCl and overnight stirring (200 rpm) at 80°C. To prepare the graphene/PVDF (G/PVDF) solutions, graphene powders were first dispersed in a certain amount of DMF for at least 2 h by bath sonication (Soniclean). After sonication, the G/DMF solution was mixed with 10 wt% PVDF powder and 3 wt% LiCl by stirring (200 rpm) at 80°C for 24 hours. Afterwards, the neat PVDF and G/PVDF solutions were further stirred (150 rpm) at 30°C for at least 72 hours. The solution composition used in this study is listed in Table 1. Hereinafter, G/PVDF-x refers to graphene/PVDF membrane with graphene concentration of x wt%. For instance, G/PVDF-0.1 indicates composite membrane with 0.1 wt% graphene content.

(Table 1)

2.3 Fabrication of G/PVDF flat-sheet membrane by phase inversion (casting)

A certain amount of neat PVDF or G/PVDF solution was poured over a glass plate and was gently lathered by a casting knife at a gap of 300 μm. Then, the lathered film solution was immediately immersed into a coagulation bath (DI water) for 1 h. After completing coagulation, the membrane was transferred and immersed into another coagulation bath (DI water) for 24 h to remove

the residual solvents, and afterwards, it was rinsed with DI water, followed by drying in the air at room temperature until a dry flat-sheet membrane was obtained.

2.4 Characterization and measurements

2.4.1. Morphology

The surface and cross-sectional morphologies of the fabricated membranes were observed by scanning electron microscopy (SEM, Zeiss Supra 55VP, Carl Zeiss AG) and energy dispersive x-ray spectroscopy (EDX). Samples taken from each membrane were first lightly coated with Au/Pd. The SEM imaging was carried out at an accelerating voltage of 10 kV, and multiple image magnifications at various areas were taken for each sample.

2.4.2. Contact angle

The membrane contact angle (CA) was measured by the sessile drop method using an optical subsystem (Theta Lite 100) integrated with an image-processing software. Sample membranes were placed on a platform, and droplets of 5-8 µL were dropped carefully on the membrane surface. A real-time camera captured the image of the droplet, and the CA was estimated by a computer. At least 5 measurements were taken for each membrane sample and the average value is reported here.

2.4.3. Surface roughness

Membrane surface roughness was analyzed by atomic force microscopy (AFM) imaging. AFM was carried out under ambient conditions in non-contact mode with silicon probes (Dimension 3100 Scanning Probe Microscope, Bruker). All membranes were scanned three times, and each time the scan position was randomly selected [24, 25].

2.4.4. Porosity

The membrane porosity, defined as the volume of pores divided by the total volume of the membrane, was measured via a gravimetric method [7]. Membrane samples with equal sizes of 2 cm

× 2 cm were immersed in ethanol (Scharlau). The weight of the samples was measured before and after saturation of ethanol, and the membrane porosity was determined by the following equation:

$$\varepsilon = \frac{(W_1 - W_2)/D_e}{[(W_1 - W_2)/D_e] + W_2/D_p} \quad (1)$$

2.4.5. Liquid entry pressure

Liquid entry pressure (LEP) is the minimum pressure required to enable water to penetrate the membrane pores. LEP is affected by the membrane hydrophobicity, maximum pore size and pore shape, and can be calculated using the Laplace equation [26]. In the present study, the LEP of the membrane was obtained using a home-made LEP apparatus as shown schematically in Figure 1. The reservoir was first filled with 25 mL distilled water and then a dry membrane sample (effective surface area = 7 cm^2) was tightly secured in the cell. Nitrogen gas was then supplied through the bottom of the water-filled chamber, raising the pressure step wise thereby pushing the water up to the membrane sample. The first sign of water bubble on the top of the membrane was regarded as the LEP. To reduce the error, triplicate measurements were taken and averaged.

(Figure 1)

2.4.6. Solution viscosity

Solution viscosity was measured using a rotational rheometer (LVF model, Brookfiled). A motor speed was selected and the spindle was allowed to rotate for 3 ~ 5 min until the monitor on the dial attained a constant value. Seven measurements per solution were performed and the average and standard deviations were reported.

2.4.7. Pore size and pore size distribution

The mean pore size of the commercial and fabricated membranes was measured by capillary flow porometry (Porolux 1000). All samples were first applied with N_2 gas to determine the gas permeability. Then the dry samples were wetted by Porefil (a wetting liquid with a low surface

tension of 16 dynes/cm) and tested under the same condition. The mean pore size of the samples was calculated at wet, dry, and half dry conditions.

2.4.8. Tensile property

The mechanical properties of the different membrane samples were measured using a Universal Testing Machine (UTM LS, Lloyd) equipped with a 1 kN load cell. The test was conducted using a constant elongation velocity of 5 mm/min under room temperature.

2.4.9. X-ray diffraction

X-Ray diffraction (XRD) (Siemens D5000) was carried out over Bragg angles ranging from 10° to 50° (Cu Kα, λ=1.54059Å).

2.5 Evaluation of membrane performance by AGMD

The commercial and fabricated membranes were tested in a home-made AGMD set-up with an effective membrane area of 21 cm^2 and a feed channel dimension of 60 mm × 35 mm × 1 mm (L × W × H) (Fig. 2). The thickness of the air gap was 3 mm. The coolant plate was made of a stainless steel (SUS-316L) to condense the water vapor and produce pure water. The AGMD in a co-current flow set-up was carried out with constant inlet temperatures at the feed and the coolant sides of 60.0 ± 1.5°C and 20.0 ± 1.5°C, respectively. The feed solution was real RO brine from CSG produced water (from Gloucester Basin located along the lower north coast of New South Wales, Australia) with conductivity and TDS concentration of around 21.8 mS/cm and 14,000 mg/L, respectively [3], and the coolant fluid was tap water. Key characteristics of this CSG RO brine are available elsewhere [3]. The feed and coolant circulation rates were both maintained at 24 L/h. The inlet and outlet temperatures on both feed and coolant sides were measured by thermocouples. The concentration of the feed and permeate water was constantly measured with electrical conductivity meters (HQ40d, Hach) throughout the tests. A commercial PVDF flat-sheet membrane (pore size = 0.22 μm, Durapore®-GVHP, Millipore) was used for comparison. The permeate flux was calculated according to the following equation:

$$J\ (L/m^2h) = \frac{\Delta g}{A \cdot t} \quad (2)$$

where, J, Δg, A and t represent the water permeate flux (L/m^2h or LMH), mass of permeate (L), effective area of the membrane (m^2) and operating duration (h), respectively. The normalized flux was calculated according to the following equation [27]:

$$J/J_o\ (\%) = \frac{Flux_E}{Flux_I} \times 100 \quad (3)$$

where, $Flux_E$ and $Flux_I$ are the flux at a specific point and the flux of the initial point, respectively. The equation used to calculate the rejection was as follows:

$$RE\ (\%) = \frac{C_I - C_F}{C_I} \times 100 \quad (4)$$

(Figure 2)

3. Results and discussion

3.1 Effect of graphene loading on membrane characteristics

3.1.1. Membrane morphology and structure

Figure 3 shows the representative SEM images of the top and bottom surfaces and cross-section views of the fabricated membranes. Based from the figure, it can be observed that the incorporation of graphene has affected the morphology of the resultant membrane wherein the presence of graphene resulted to more dense top surface (Fig. 3b1-g1). However, the bottom surfaces showed bigger pore sizes for the graphene-embedded membranes compared to neat PVDF, wherein the loading at 0.5 wt% showed uniformly distributed pores (Fig. 3a2-g2). However, at graphene loading of >0.5 wt%, the bottom surfaces tend to become much denser with decreasing number of pores. Cross-section images of all membranes (Fig. 3a3-g3) reveal typical asymmetric structure, i.e., a thin dense top surface with no open pores and a porous sub-layer/bulk morphology. Neat PVDF depicted finger-like structure near the top and distributed macro-voids going to the bottom surface. More elongated finger-like macro-voids were observed for the graphene-loaded membranes up to 0.5 wt%, wherein the 0.5 wt% graphene loading showed larger and straighter finger-like pores, but at higher loading than that, the bulk of the structure tends to be less elongated and turned to sponge-like

macrovoids. This SEM observation is consistent with the increase in mean pore size and porosity of the membrane up to 0.5 wt%, and then slightly decreased at higher loadings (Table 2). The highest porosity and pore size was observed for G/PVDF-0.5 membrane at 84.7% and 0.11 μm, respectively. The phase inverted membranes also presented higher porosity (78.2 to 84.7%) but at smaller mean pore sizes (0.03 to 0.11 μm) compared to C-PVDF membrane (70.3% and 0.22 μm, respectively) [28].

(Figure 3)

Figure 4 shows that casting solution viscosity increased slightly from 420 to 470 cP as graphene concentration increased to 0.7 wt%. Thereafter, a significant increase in viscosity was observed as the graphene concentration continued to increase to 2 wt%. High casting solution viscosity due to a high graphene loading may have retarded the solvent/non-solvent demixing process and consequently the phase separation rate leading to sponge-like structure at higher graphene loadings [25]. In addition, the likely aggregation of graphene due to their strong hydrophobicity and van der Waal's attraction at higher loading could have also affected the resulting viscosity and morphology of the membrane. The van der Waal's interacted between each graphene nanoparticles and the C – C bonds by jointing C dangling bonds of other graphene nanoparticles [29]. Thus, the more tendency of graphene to aggregate at higher loadings (0.7 to 2.0 wt%) resulted to the decrease in pore sizes. On the other hand, the lower viscosity from 0.1 to 0.5 wt% enables the acceleration of water entry to the membranes, which resulted in fast exchange between the solvent and non-solvent [25] leading to more elongated finger-like structure. The thickness of the graphene/PVDF membranes (Table 2) also increased with increasing graphene loading (from 82.8 μm for neat PVDF to 98.4 μm for 2 wt% graphene/PVDF). This observed thickness increase is primarily attributed to the increase in solution viscosity and the addition of more graphene [30].

(Figure 4)

The presence of graphene in the membrane was examined by EDX and XRD analysis. It is expected that graphene addition would increase the membrane carbon content if graphene is well dispersed in the membrane. Figure 5(a) shows increasing carbon/fluorine (C/F) ratio with increasing graphene loading confirming the successful incorporation of graphene in the composite membrane. Visual inspection showed darker color for G/PVDF membranes compared to neat PVDF mainly due to the presence of graphene (images not shown). XRD patterns (Fig. 5(b)) also reveal new peak at 2θ = 26.7º (0 0 2) [31] for the G/PVDF membranes, which is attributed to the presence of graphene. Both neat and G/PVDF membranes showed peaks at 18.5º and 36.3º corresponding to α-crystalline phase (0 2 0) and at 20.5º indicating β-crystalline phase (2 0 0)/(1 1 0) of PVDF [32].

(Figure 5)

(Table 2)

3.1.2. Membrane contact angle

The surface contact angle of the fabricated membranes was measured with DI water by a sessile drop method. The CA at the top surface increased from 73.8 ± 1.5°, to 78.0 ± 1.6, 80.6 ± 0.6, 87.2 ± 2.5, 91.7 ± 1.2, 96.5 ± 1.1 and 103.3 ± 2.0° as the concentration of graphene was increased from 0 to 0.1, 0.3, 0.5, 0.7, 1.0 and 2.0 wt%, respectively (Table 2). This increase is attributed to the presence of hydrophobic graphene in the composite membrane, wherein more graphene is exposed at the surface at higher concentration. Checking the surface roughness of the membranes by AFM (Fig. 6) reveals quite similar mean roughness (23-27 nm) for all membranes, with slight increase at much higher graphene loading (1 and 2 wt%), which could be due to some agglomeration at that loading range. The G/PVDF-0.5 membrane posted slightly lower R_a but still high CA, which was maybe because of the good finger-like structure morphology of the membrane due to the fast exchange between the solvent and non-solvent leading to smoother surface [25]. It should be noted that the fabricated phase inverted membranes with graphene have much lower surface roughness (17-28 nm)

compared with the commercial PVDF membrane (145 nm, AFM image not shown here), which could have led to C-PVDF having higher hydrophobicity.

(Figure 6)

3.1.3. Membrane liquid entry pressure

In MD, liquid water is prevented from penetrating the membrane by the water – membrane surface tension and a hydrophobic membrane is usually used. Membrane wetting potential can be determined by LEP, which is the minimum pressure for liquid water to penetrate the pores of the membrane, usually at least 1.5 bar to prevent membrane wetting. A high LEP value is important for long term MD performance. LEP is affected by the hydrophobicity of the material, maximum pore size and shape according to the Laplace equation. In the present study, the neat PVDF posted an LEP of 2.16 bar, which is very similar with that of C-PVDF (2.13 bar, GVHP membrane) (Table 2). The addition of different loadings of graphene in the membrane has resulted to increasing LEP values from 3.66 bar for G/PVDF-0.1 to as high as 7.84 bar for G/PVDF-2.0. This increase is attributed to the smaller mean pore sizes of the G/PVDF membranes as well as to the increased membrane hydrophobicity at higher graphene loading. Moreover, the less porous structure of the bulk and the bottom surfaces of loadings >0.5 wt% has also contributed to the higher LEP. The LEPs of the present G/PVDF membranes are deemed suitable for MD process.

3.1.4. Membrane tensile properties

The tensile properties of the G/PVDF and neat membranes are shown in Table 2. Incorporation of increasing graphene concentration resulted to increasing tensile strength (4.1 to 6.0 MPa compared to 3.5 MPa for neat membrane). This confirms good dispersion of graphene in the PVDF membrane that led to good load transfer from PVDF to graphene resulting to enhanced tensile strength. In addition, the structure of the membrane itself has also affected the tensile properties. In general, a finger-like structure membrane has lower tensile strength than a sponge-like structure membrane [33]. Looking at the SEM images in Fig. 3, G/PVDF-0.7 to G/PVDF-2.0 exhibited sponge-

like structure and together with the added effect of graphene, has resulted to increased tensile strength. Neat PVDF also revealed sponge-like structure, but still it was lower in tensile strength compared to G/PVDF-0.1 to G/PVDF-0.5 even though the latter membranes have finger-like structure, primarily because of the added effect of graphene incorporation that strengthens the composite membranes [21]. Interestingly, the elongation at break also correspondingly increased up to a loading of 0.7 wt%, but beyond that, it started to decrease but still higher than the neat membrane. This could be due to some agglomeration at higher graphene content.

3.2 Air gap membrane distillation (AGMD) performance of the fabricated membranes

3.2.1 Effect of graphene concentration

The effect of different loadings of graphene onto the phase inverted PVDF membrane to the flux and salt rejection performance in AGMD mode was investigated. AGMD tests were carried out for 24 h of operation at feed and coolant inlet temperatures of 60 and 20 ^{o}C, respectively using RO brine from CSG produced water as feed (Fig. 7). Results indicated increasing flux performance from 11.6 LMH for neat membrane to 15.3, 18.5 and 20.5 LMH for G/PVDF-0.1, G/PVDF-0.3 and G/PVDF-0.5, respectively and then started to decrease beyond 0.5 wt% graphene loading (19.5, 18.2 and 15.8 LMH for 0.7, 1.0 and 2.0 wt% graphene loading). This increasing trend is attributed to the favorable membrane properties at this graphene loading range (0.1 to 0.5 wt%). As presented in Table 2, though higher hydrophobicity was obtained for loading >0.5 wt%, the pore size and porosity were drastically decreased, while the thickness was increased leading to the decrease in permeate flux. The loadings from 0.1 wt% to 0.5, having a combination of increasing pore sizes and porosity, and thinner thickness, have contributed to the increased flux. It should be noted that the flux is directly proportional to the pore size and porosity and inversely proportional to the thickness of the membrane. Larger pore size and porosity give more surface area for vapor to pass through thereby increasing the mass flux, while thinner thickness provides shorter path for vapor to travel across and has lower mass transfer resistance. In addition, the presence of graphene, which has a rapid sorption/desorption capacity, could have allowed the vapor to follow a surface diffusion pattern [34], thereby aiding in the

increase of vapor flux through the membrane. The high LEP of all the fabricated membranes resulted to almost 100% salt rejection with the final permeate conductivity of 3.4 µS/cm or lower. In the present study, the optimal graphene loading was found to be 0.5 wt%, i.e., G/PVDF-0.5 membrane showing the highest flux of 20.5 LMH and stable salt rejection of nearly 100%. Its finger-like structure and straighter pore structure (i.e., lower tortuosity), and its appropriate pore size (0.11 µm), highest porosity (85%), high LEP (3.89 bar) and adequate hydrophobicity (87.2^{o}) have all contributed to its superior AGMD performance. Clearly, the addition of graphene in the cast PVDF membrane has modified the membrane structure and enhanced the membrane properties for MD application.

(Figure 7)

3.2.2 Long-term AGMD tests of the G/PVDF and commercial membranes

For practical application, the membrane should maintain a stable performance for long term operation. In literature, only few studies have conducted long-term MD performance tests of their membranes. A suitable membrane should exhibit as high flux as possible but should also be robust enough to maintain high and stable salt rejection. In this study, the optimal G/PVDF-0.5 membrane was tested for 10 days (240 h) of continuous AGMD operation and was compared with that of a commercial PVDF membrane (C-PVDF) with RO brine from CSG produced water as feed.

Figure 8 shows the normalized flux and salt rejection performance of the two membranes at feed and coolant inlet temperatures of 60 and 20^{o}C, respectively. The initial flux of G/PVDF-0.5 and commercial membrane was 20.91 LMH and 11.32 LMH, respectively. C-PVDF membrane drastically decreased to 80% from its initial flux in the first 24 h and then steadily decreased thereafter until 51.4% normalized flux after 10 d of operation. On the other hand, G/PVDF-0.5 membrane exhibited excellent stability with almost constant flux up until 6 d of operation, then slowly decreased to 85.3% normalized flux at the end of 10 d. This signifies the much superior anti-wetting ability of the graphene-loaded membrane compared to C-PVDF. G/PVDF-0.5 also posted very stable and high salt rejection of 99.99% for the whole 10 d of operation compared to 99.96% for C-PVDF. It is interesting to note that even though the flux for C-PVDF has drastically decreased in the span of 10 d, its salt

rejection was still high enough. This means that full wetting was not happening, rather there must be some changes in the surface characteristics of the membrane.

(Figure 8)

In order to verify this, the surface of the used membrane was characterized by SEM (Fig. 9). The surface and cross-sectional SEM images of the virgin C-PVDF membrane are shown in Figure S1. Indeed, C-PVDF top surface was found to have large needle-like scale deposits of salt crystals (Fig. 9a and c), which was determined to be mainly gypsum as evidenced by XRD (Fig. S2). This explains the drastic decline in flux as the deposits have constricted the surface openings of the membrane leading to much smaller pores and decreased porosity, hence the surface area for vapor to pass through has also gotten smaller. In addition, the rapid decline in flux is due to rapid growth of crystals deposition on the membrane, which led to decreasing membrane permeability [26, 35]. On the other hand, G/PVDF-0.5 membrane showed clear surface similar with its virgin membrane surface without much trace of any deposits (Fig. 9b and d). Hence, more stable flux and salt rejection was observed. The more salt deposition on the commercial membrane could be due to the following: 1) the much rougher surface of C-PVDF (R_a = 145 nm compared to 17 nm for G/PVDF-0.5) could have provided more surface area for crystals to nucleate and deposit, as also observed by other studies suggesting that polymeric membrane surface behaves as a support to promote heterogeneous nucleation [35, 36], and (2) the bigger pore size (0.22 μm) of C-PVDF could have allowed the salt crystals to slowly penetrate the pore mouth, where additional crystal growth or precipitation occurred. Meanwhile, the much smoother surface, small pore size and high LEP of G/PVDF-0.5 could have lessen the chances of heterogeneous nucleation on the surface, and prohibit the penetration of salts into the pore depth; hence lower tendency for scaling occurred [37, 38]. Even at low flow velocity, the scales could have been constantly removed by the flow shear force thereby leaving the surface clean for longer period of time. Other studies have also indicated the anti-fouling property of graphene, which could have contributed to the lesser fouling tendency of G/PVDF-0.5. Generally, MD is regarded to have lower fouling propensity compared to pressure-driven membrane separation processes [26].

(Figure 9)

4. Conclusion

Graphene/PVDF (G/PVDF) membranes were successfully fabricated by a phase inversion method and evaluated by AGMD process using real RO brine from CSG produced water as feed. Graphene nanoparticles have been dispersed well on/in the fabricated membranes, which were confirmed by XRD and EDX. Among all the G/PVDF membranes with various graphene concentrations, G/PVDF-0.5 (i.e., 0.5 wt% graphene loading) membrane showed a suitable pore size (0.11 μm), thickness (88 μm), porosity (85%), and LEP (3.89 bar) for AGMD process. Contact angle of the G/PVDF-0.5 membrane was higher than those of G/PVDF-0.1, G/PVDF-0.3, and neat membranes due to the presence of more hydrophobic graphene although its surface roughness was slightly lower than other membranes. When graphene concentration was increased over 0.7 wt%, the fabricated membranes tended to have smaller pore size, lower porosity, thicker thickness, and higher contact angle than that of G/PVDF-0.5 membrane due to the aggregation of the graphene nanoparticle. Thus, flux of the G/PVDF-0.5 membrane was the highest among all the membranes for 24 hours of AGMD test. For 10 days AGMD test, G/PVDF-0.5 membrane showed more stable flux, better rejection performances, and lesser scaling tendency compared with commercial PVDF membrane; as well as, it was not wetted due to the enhanced membrane features and to the effect of the nature of graphene. Therefore, the present results suggest that membrane made of PVDF blended with nanoporous graphene nanoparticles has good potential as a robust MD membrane for the treatment of RO brine from CSG produced water by AGMD.

Acknowledgments

This research was supported by a grant (15IFIP-B065893-03) from the Industrial Facilities & Infrastructure Research Program funded by Ministry of Land, Infrastructure and Transport of Korean government. The authors also acknowledge the grants from the UTS Chancellor's Postdoctoral Research Fellowship, ARC Future Fellowship and UTS FEIT seed fund.

Nomenclature

A	Effective area of the membrane
C_F	Permeate concentration
C_I	Feed concentration
$Flux_E$	Flux of each point
$Flux_I$	Flux of the initial point
J	Water vapor flux
J/J_o	Normalized flux
RE	Rejection ratio
W_1	Weight of the saturated membrane
W_2	Weight of the dry membrane
t	Operating duration
Δg	Mass of permeate
ε	Membrane porosity
ρ	Liquid density
D_e	Density of ethanol
D_p	Density of PVDF material

Abbreviation

2D	Two-dimensional
AFM	Atomic force microscopy
AGMD	Air gap membrane distillation
CA	Contact angle
CSG	Coal seam gas

DCMD	Direct contact membrane distillation
DI	De-ionized
DMF	N, N-dimethylformamide
EDX	Energy dispersive x-ray spectroscopy
G/PVDF	Graphene/PVDF
LEP	Liquid entry pressure
LiCl	Lithium chloride
MD	Membrane distillation
MF	Microfiltration
NaCl	Sodium chloride
PVDF	Polyvinylidene fluoride
RO	Reverse Osmosis
SEM	Scanning electron microscopy
VMD	Vacuum membrane distillation
XRD	X-ray diffraction

References

[1] L.D. Nghiem, C. Elters, A. Simon, T. Tatsuya, W. Price, Coal seam gas produced water treatment by ultrafiltration, reverse osmosis and multi-effect distillation: A pilot study, Separation and Purification Technology, 146 (2015) 94-100.

[2] L.D. Nghiem, T. Ren, N. Aziz, I. Porter, G. Regmi, Treatment of coal seam gas produced water for beneficial use in Australia: A review of best practices, Desalination and Water Treatment, 32 (2011) 316-323.

[3] H.C. Duong, A.R. Chivas, B. Nelemans, M. Duke, S. Gray, T.Y. Cath, L.D. Nghiem, Treatment of RO brine from CSG produced water by spiral-wound air gap membrane distillation — A pilot study, Desalination, 366 (2015) 121-129.

[4] S. Mondal, S.R. Wickramasinghe, Produced water treatment by nanofiltration and reverse osmosis membranes, Journal of Membrane Science, 322 (2008) 162-170.

[5] H.C. Duong, S. Gray, M. Duke, T.Y. Cath, L.D. Nghiem, Scaling control during membrane distillation of coal seam gas reverse osmosis brine, Journal of Membrane Science, 493 (2015) 673-682.

[6] I. Hamawand, T. Yusaf, S.G. Hamawand, Coal seam gas and associated water: A review paper, Renewable and Sustainable Energy Reviews, 22 (2013) 550-560.

[7] L.D. Tijing, Y.C. Woo, M.A.H. Johir, J.-S. Choi, H.K. Shon, A novel dual-layer bicomponent electrospun nanofibrous membrane for desalination by direct contact membrane distillation, Chemical Engineering Journal, 256 (2014) 155-159.

[8] L.D. Tijing, Y.C. Woo, W.-G. Shim, T. He, J.-S. Choi, S.-H. Kim, H.K. Shon, Superhydrophobic nanofiber membrane containing carbon nanotubes for high-performance direct contact membrane distillation, Journal of Membrane Science, 502 (2016) 158-170.

[9] L.D. Nghiem, F. Hildinger, F.I. Hai, T. Cath, Treatment of saline aqueous solutions using direct contact membrane distillation, Desalination and Water Treatment, 32 (2011) 234-241.

[10] S. Nejati, C. Boo, C.O. Osuji, M. Elimelech, Engineering flat sheet microporous PVDF films for membrane distillation, Journal of Membrane Science, 492 (2015) 355-363.

[11] M. Tian, Y. Yin, C. Yang, B. Zhao, J. Song, J. Liu, X.-M. Li, T. He, CF4 plasma modified highly interconnective porous polysulfone membranes for direct contact membrane distillation (DCMD), Desalination, 369 (2015) 105-114.

[12] M. Sadrzadeh, S. Bhattacharjee, Rational design of phase inversion membranes by tailoring thermodynamics and kinetics of casting solution using polymer additives, Journal of Membrane Science, 441 (2013) 31-44.

[13] J.A. Prince, G. Singh, D. Rana, T. Matsuura, V. Anbharasi, T.S. Shanmugasundaram, Preparation and characterization of highly hydrophobic poly(vinylidene fluoride) – Clay

nanocomposite nanofiber membranes (PVDF–clay NNMs) for desalination using direct contact membrane distillation, Journal of Membrane Science, 397-398 (2012) 80-86.

[14] D. Hou, G. Dai, H. Fan, J. Wang, C. Zhao, H. Huang, Effects of calcium carbonate nano-particles on the properties of PVDF/nonwoven fabric flat-sheet composite membranes for direct contact membrane distillation, Desalination, 347 (2014) 25-33.

[15] M. Baghbanzadeh, D. Rana, T. Matsuura, C.Q. Lan, Effects of hydrophilic CuO nanoparticles on properties and performance of PVDF VMD membranes, Desalination, 369 (2015) 75-84.

[16] T.L.S. Silva, S. Morales-Torres, J.L. Figueiredo, A.M.T. Silva, Multi-walled carbon nanotube/PVDF blended membranes with sponge- and finger-like pores for direct contact membrane distillation, Desalination, 357 (2015) 233-245.

[17] S. Roy, M. Bhadra, S. Mitra, Enhanced desalination via functionalized carbon nanotube immobilized membrane in direct contact membrane distillation, Separation and Purification Technology, 136 (2014) 58-65.

[18] L. Zhao, X. Lu, C. Wu, Q. Zhang, Flux enhancement in membrane distillation by incorporating AC particles into PVDF polymer matrix, Journal of Membrane Science, 10.1016/j.memsci.2015.11.010 (2015).

[19] K. Celebi, J. Buchheim, R.M. Wyss, A. Droudian, P. Gasser, I. Shorubalko, J.-I. Kye, C. Lee, H.G. Park, Ultimate Permeation Across atomically thin porous graphene, Science, 344 (2014) 289.

[20] R. Moradi, J. Karimi-Sabet, M. Shariaty-Niassar, M. Koochaki, Preparation and Characterization of Polyvinylidene Fluoride/Graphene Superhydrophobic Fibrous Films, Polymers, 7 (2015) 1444-1463.

[21] F. Perreault, A. Fonseca de Faria, M. Elimelech, Environmental applications of graphene-based nanomaterials, Chem Soc Rev, 44 (2015) 5861-5896.

[22] M. Bhadra, S. Roy, S. Mitra, Desalination across a graphene oxide membrane via direct contact membrane distillation, Desalination, 378 (2016) 37-43.

[23] E.O. Polat, O. Balci, N. Kakenov, H.B. Uzlu, C. Kocabas, R. Dahiya, Synthesis of Large Area Graphene for High Performance in Flexible Optoelectronic Devices, Scientific Reports, 5 (2015) 16744.

[24] Y. Kim, S. Lee, J. Kuk, S. Hong, Surface chemical heterogeneity of polyamide RO membranes: Measurements and implications, Desalination, 367 (2015) 154-160.

[25] M.J. Park, S. Phuntsho, T. He, G.M. Nisola, L.D. Tijing, X.-M. Li, G. Chen, W.-J. Chung, H.K. Shon, Graphene oxide incorporated polysulfone substrate for the fabrication of flat-sheet thin-film composite forward osmosis membranes, Journal of Membrane Science, 493 (2015) 496-507.

[26] L.D. Tijing, Y.C. Woo, J.-S. Choi, S. Lee, S.-H. Kim, H.K. Shon, Fouling and its control in membrane distillation—A review, Journal of Membrane Science, 475 (2015) 215-244.

[27] Y.C. Woo, J.J. Lee, L.D. Tijing, H.K. Shon, M. Yao, H.-S. Kim, Characteristics of membrane fouling by consecutive chemical cleaning in pressurized ultrafiltration as pre-treatment of seawater desalination, Desalination, 369 (2015) 51-61.

[28] Y.C. Woo, L.D. Tijing, M.J. Park, M. Yao, J.-S. Choi, S. Lee, S.-H. Kim, K.-J. An, H.K. Shon, Electrospun dual-layer nonwoven membrane for desalination by air gap membrane distillation, Desalination, 10.1016/j.desal.2015.09.009 (2015).

[29] Y. Yang, W. Rigdon, X. Huang, X. Li, Enhancing graphene reinforcing potential in composites by hydrogen passivation induced dispersion, Sci Rep, 3 (2013) 2086.

[30] D. Hou, H. Fan, Q. Jiang, J. Wang, X. Zhang, Preparation and characterization of PVDF flat-sheet membranes for direct contact membrane distillation, Separation and Purification Technology, 135 (2014) 211-222.

[31] Q. An, F. Lv, Q. Liu, C. Han, K. Zhao, J. Sheng, Q. Wei, M. Yan, L. Mai, Amorphous vanadium oxide matrixes supporting hierarchical porous Fe3O4/graphene nanowires as a high-rate lithium storage anode, Nano Lett, 14 (2014) 6250-6256.

[32] C.L. Yang, Z.H. Li, W.J. Li, H.Y. Liu, Q.Z. Xiao, G.T. Lei, Y.H. Ding, Batwing-like polymer membrane consisting of PMMA-grafted electrospun PVdF–SiO2 nanocomposite fibers for lithium-ion batteries, Journal of Membrane Science, 495 (2015) 341-350.

[33] P.V.d. Witte, P.J. Dijkstra, J.W.A.V.d. Berg, J. Feijen, Phase separation processes in polymer solutions in relation to membrane formation, Journal of Membrane Science, 117 (1996) 1-31.

[34] S.P. Surwade, S.N. Smirnov, I.V. Vlassiouk, R.R. Unocic, G.M. Veith, S. Dai, S.M. Mahurin, Water desalination using nanoporous single-layer graphene, Nat Nanotechnol, 10 (2015) 459-464.

[35] C.M. Tun, A.G. Fane, J.T. Matheickal, R. Sheikholeslami, Membrane distillation crystallization of concentrated salts—flux and crystal formation, Journal of Membrane Science, 257 (2005) 144-155.

[36] S. Fermani, G. Falini, M. Minnucci, A. Ripamonti, Protein crystallization on polymeric film surfaces, Journal of Crystal Growth, 224 (2001) 327-334.

[37] V. Vatanpour, S.S. Madaeni, R. Moradian, S. Zinadini, B. Astinchap, Fabrication and characterization of novel antifouling nanofiltration membrane prepared from oxidized multiwalled carbon nanotube/polyethersulfone nanocomposite, Journal of Membrane Science, 375 (2011) 284-294.

[38] P. Daraei, S.S. Madaeni, N. Ghaemi, M.A. Khadivi, B. Astinchap, R. Moradian, Enhancing antifouling capability of PES membrane via mixing with various types of polymer modified multi-walled carbon nanotube, Journal of Membrane Science, 444 (2013) 184-191.

Figure list:

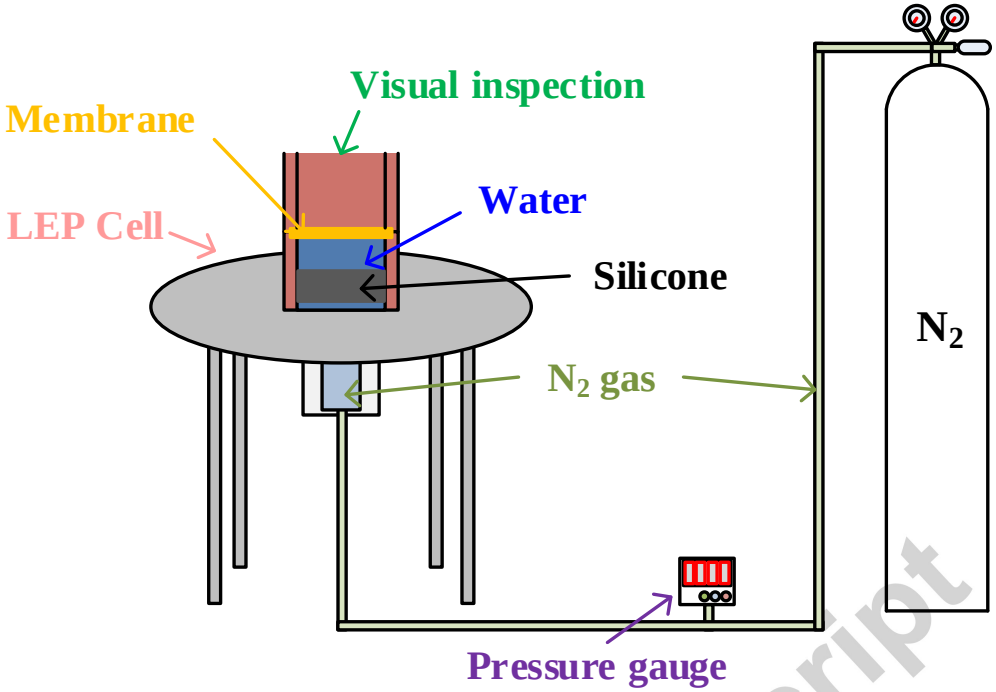

Figure 1 Schematic lay-out of the LEP apparatus.

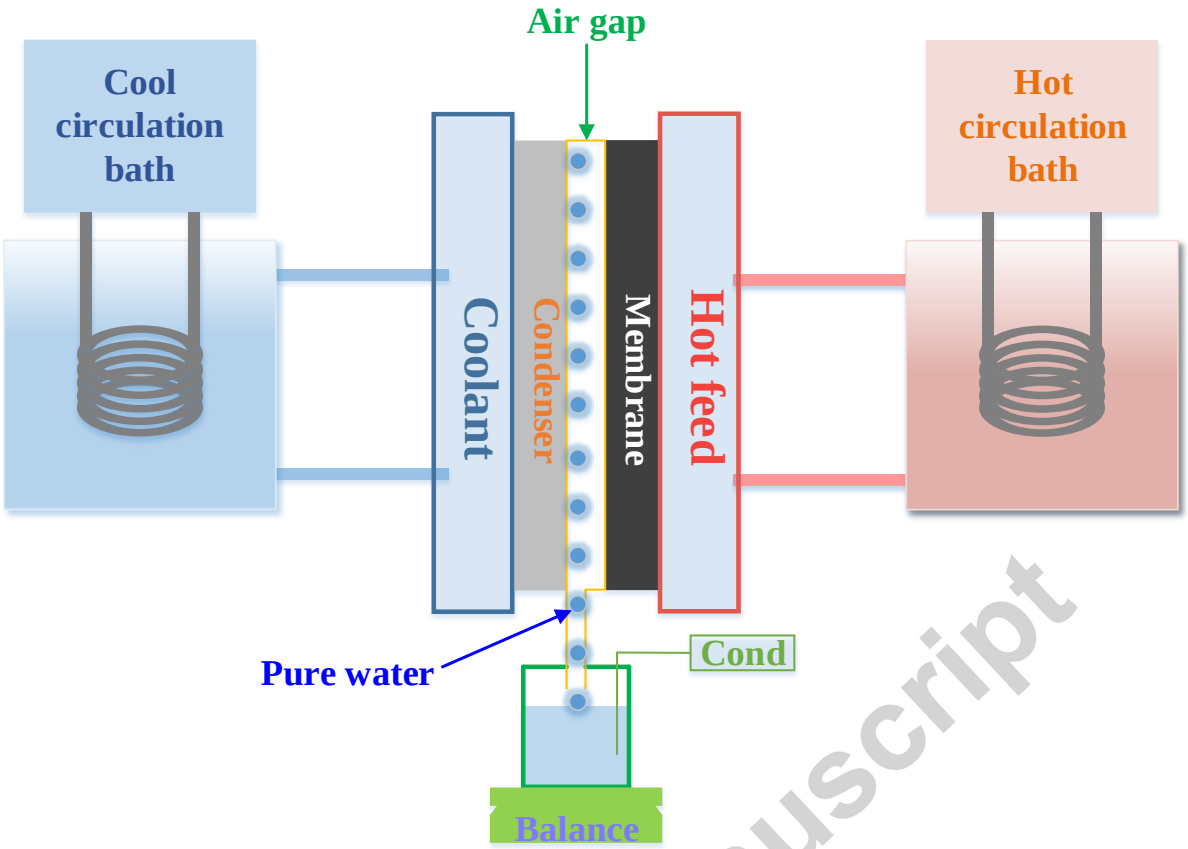

Figure 2 Schematic diagram of the AGMD system used in the present study.

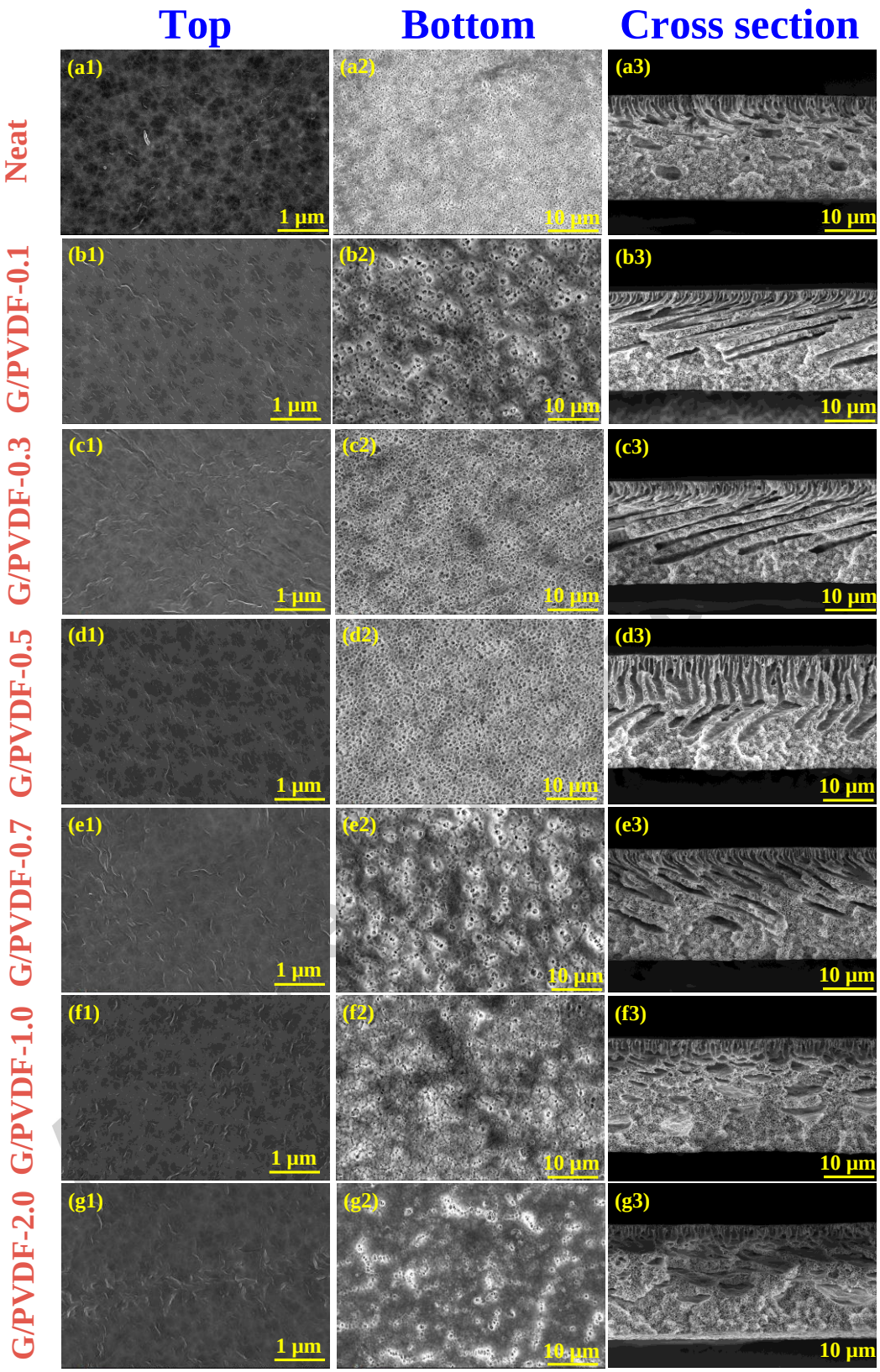

Figure 3 SEM images of the G/PVDF and neat PVDF membranes: top surface (a1 – g1), bottom surface (a2 – g2) and cross section (a3 – g3).

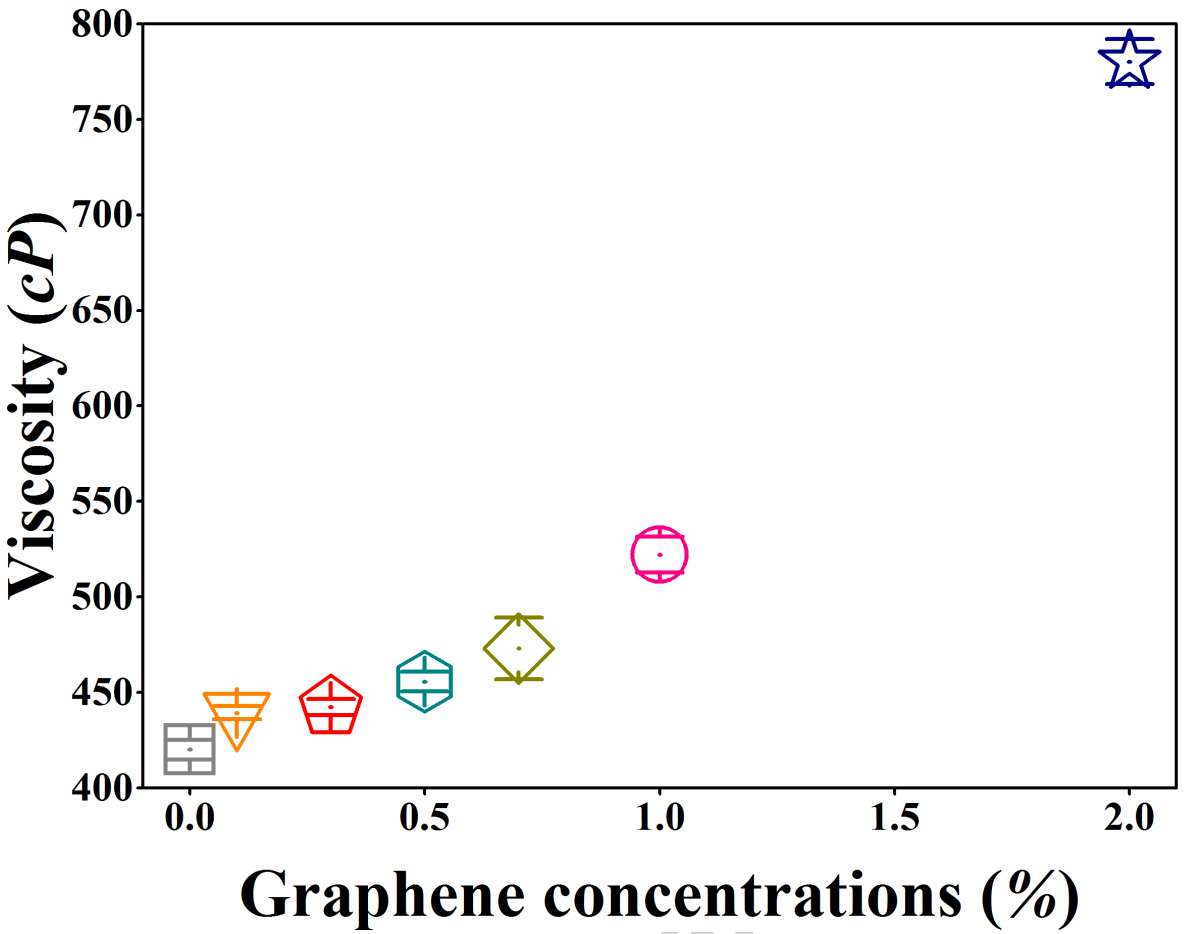

Figure 4 Viscosity measurements of the PVDF solutions at various graphene concentrations.

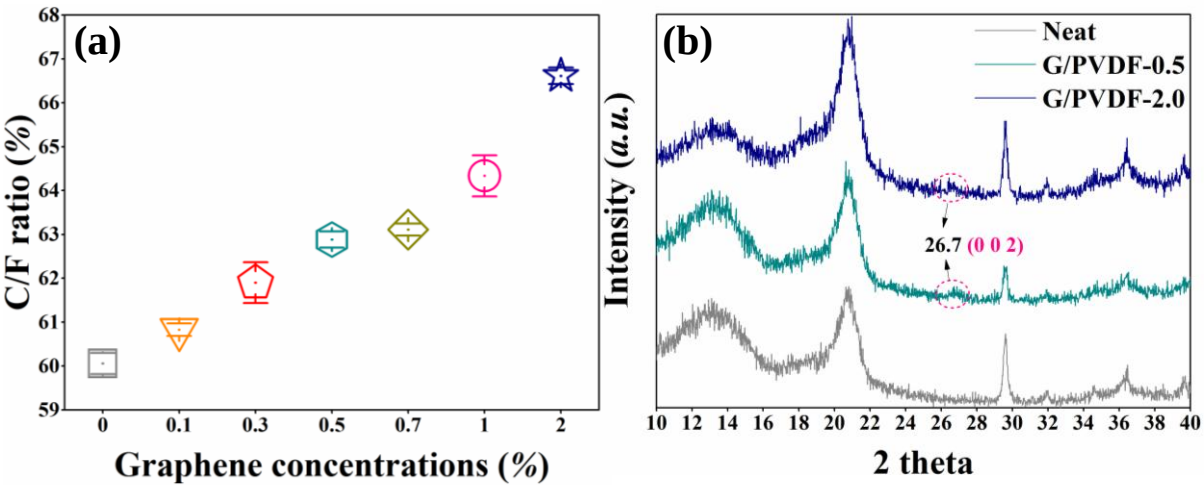

Figure 5 (a) Carbon/fluorine (C/F) ratio by EDX and (b) XRD patterns of the G/PVDF and neat PVDF membranes.

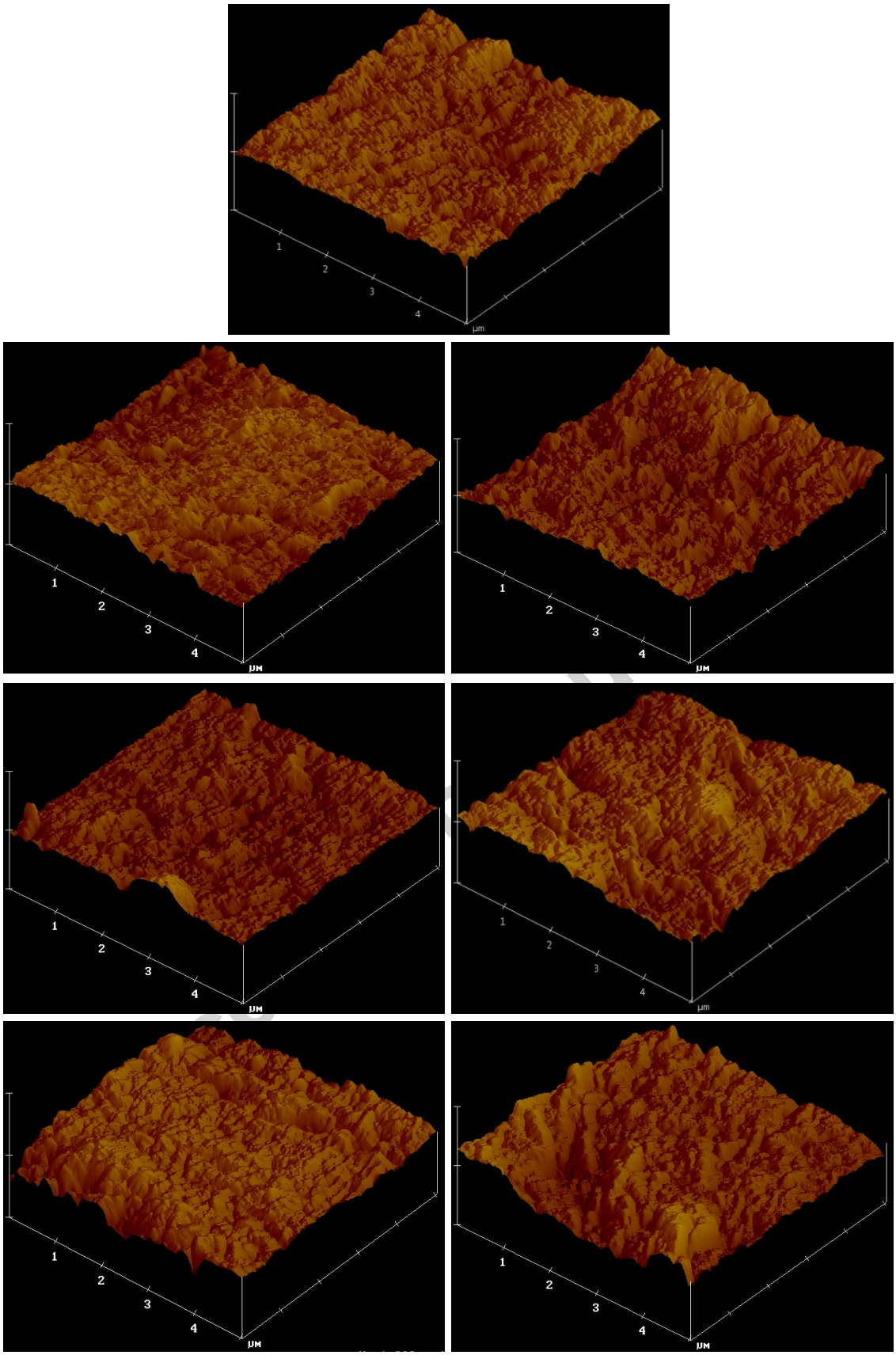

Figure 6 AFM images of the G/PVDF and neat membranes: (a) neat, (b) G/PVDF-0.1, (c) G/PVDF-0.3, (d) G/PVDF-0.5, (e) G/PVDF-0.7, (f) G/PVDF-1.0 and (g) G/PVDF-2.0.

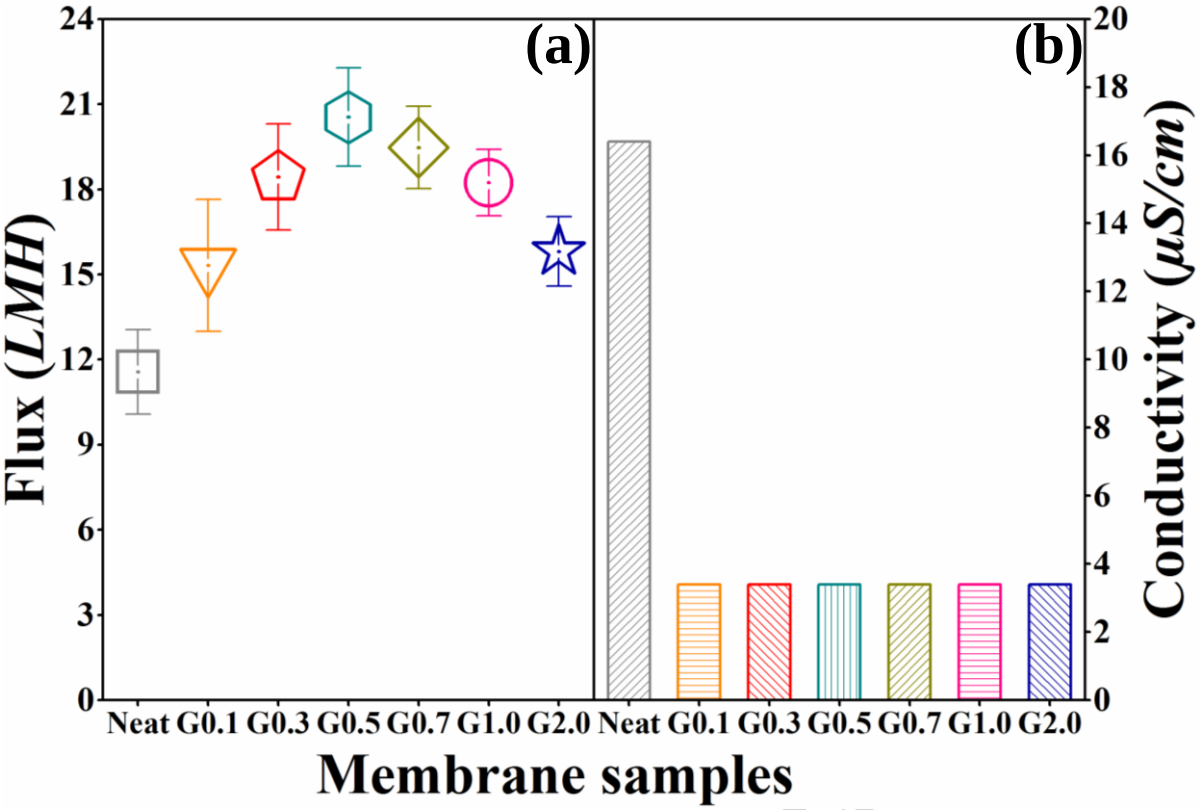

Figure 7 AGMD (a) flux and (b) the final conductivity performances of the G/PVDF and neat phase inversion membranes for 24 h operation.

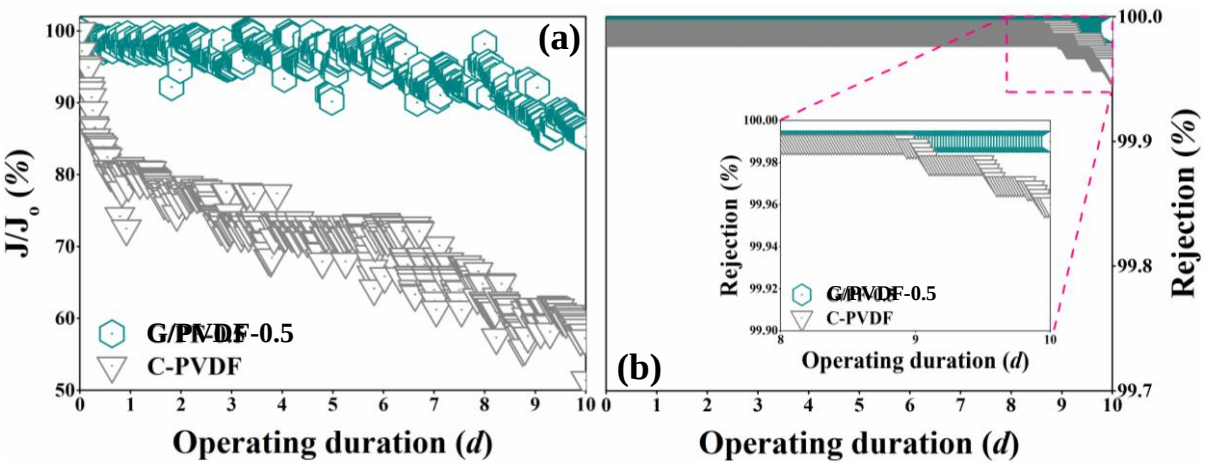

Figure 8 (a) Normalized flux and (b) salt rejection ratio performances of the G/PVDF-0.5 and commercial membranes for 10-day long term operation.

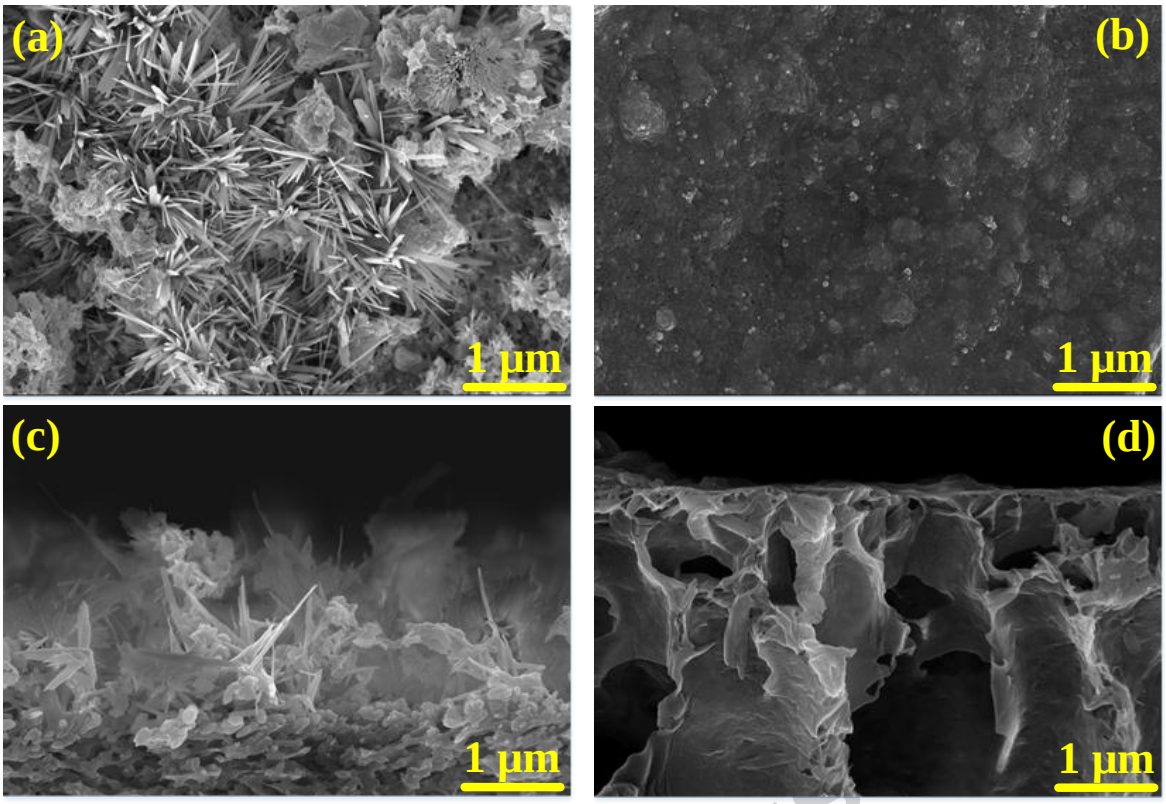

Figure 9 Surface and cross-sectional SEM images of (a, c) C-PVDF and (b, d) G/PVDF-0.5 membranes after 10 d AGMD test with RO brine from CSG produced water as feed.

Graphical abstract

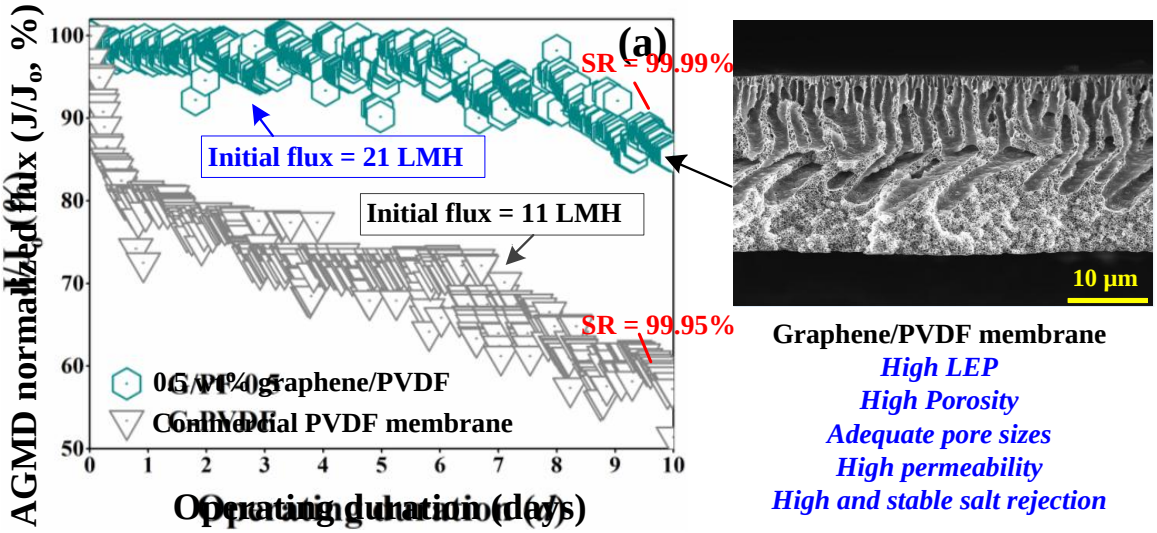

Graphene/PVDF membrane

High LEP

High Porosity

Adequate pore sizes

High permeability

High and stable salt rejection

Table list:

Table 1 Solution composition used in the present study.

Table 2 Characteristics of the G/PVDF and neat membranes used in this study.

Table 1 Solution composition used in the present study.

Membrane code	Graphene content (wt%)	Polymer	Additive	Solvent
Neat	0	10 wt% PVDF	3 wt% LiCl	87 wt% DMF
G/PVDF-0.1	0.1	10 wt% PVDF	3 wt% LiCl	87 wt% DMF
G/PVDF-0.3	0.3	10 wt% PVDF	3 wt% LiCl	87 wt% DMF
G/PVDF-0.5	0.5	10 wt% PVDF	3 wt% LiCl	87 wt% DMF
G/PVDF-0.7	0.7	10 wt% PVDF	3 wt% LiCl	87 wt% DMF
G/PVDF-1.0	1.0	10 wt% PVDF	3 wt% LiCl	87 wt% DMF
G/PVDF-2.0	2.0	10 wt% PVDF	3 wt% LiCl	87 wt% DMF

Table 2 Characteristics of the G/PVDF and neat membranes used in this study.

Membrane code	Mean pore size (μm)	Maximum pore size (μm)	Membrane Thickness (μm)	Porosity (%)	Contact angle (deg)	LEP (bar)	Tensile strength (MPa)	Elongation at break (%)
Neat	0.06 ± 0.01	0.08 ± 0.01	82.8 ± 0.9	78.2 ± 2.4	73.8 ± 1.5	2.16 ± 0.57	3.5 ± 0.6	22.0 ± 9.4
G/PVDF-0.1	0.07 ± 0.01	0.11 ± 0.02	84.2 ± 1.6	81.3 ± 1.8	78.0 ± 1.6	3.66 ± 0.15	4.1 ± 0.1	35.5 ± 3.0
G/PVDF-0.3	0.08 ± 0.01	0.12 ± 0.02	86.0 ± 0.7	83.4 ± 2.5	80.6 ± 0.6	3.72 ± 0.18	4.4 ± 0.5	60.1 ± 7.6
G/PVDF-0.5	0.11 ± 0.01	0.14 ± 0.01	88.1 ± 0.6	84.7 ± 1.1	87.2 ± 2.5	3.89 ± 0.08	5.3 ± 1.6	86.6 ± 7.3
G/PVDF-0.7	0.08 ± 0.01	0.12 ± 0.03	91.0 ± 1.2	82.6 ± 3.1	91.7 ± 1.2	4.12 ± 0.11	5.5 ± 0.5	90.1 ± 6.4
G/PVDF-1.0	0.05 ±	0.07 ± 0.01	94.3 ± 1.4	80.4 ± 1.3	96.5 ± 1.1	6.12 ±	5.7 ± 0.6	71.9 ± 3.0

	0.01					0.31		
G/PVDF-2.0	0.03 ± 0.01	0.04 ± 0.01	98.4 ± 1.7	78.9 ± 0.5	103.3 ± 2.0	7.84 ± 0.42	6.0 ± 1.6	67.9 ± 4.7
C-PVDF [36]	0.22 ± 0.09	0.29 ± 0.11	107.4 ± 1.6	70.3 ± 0.3	131.1 ± 3.1	2.13 ± 0.02	7.2 ± 0.2	36.3 ± 3.1

Highlights

- PVDF membranes were fabricated by phase inversion for CSG RO brine treatment by AGMD.
- Effect of graphene loading on membrane properties and performance was investigated.
- Optimal graphene loading resulted to high LEP and porosity, and adequate pore size.
- Incorporation of small amount of graphene improved the AGMD performance.
- G/PVDF membranes presented excellent flux and performance stability for 10 days.